Proceedings of IMECE2007
2007 ASME International Mechanical Engineering Congress and Exposition
November 11-15, 2007, Seattle, Washington, USA

IMECE2007-42037

SIMULATION-BASED ANALYSIS OF 3D FLOW INSIDE A MICROPUMP WITH PASSIVE VALVES

A. F. Tabak[a,1], A. Solak[a,2], E.Y. Erdem[b,3], C. Akcan[a,4], S. Yesilyurt[a,5]

[a]Sabanci University Tuzla
Istanbul, Turkey

{[1]tabak,[2]altugs,[3]yeganerdem,
[4]canerakcan}@su.sabanciuniv.edu
[5]syesilyurt@sabanciuniv.edu

[b]University of Washington
College of Engineering
Loew Hall
Seattle, Washington

ABSTRACT

It is expected that chemical, biological and environmental applications of microdevices will increase with new developments in micromachining techniques. In this work, a micropump design that utilizes passive valves and an actuated diaphragm is presented. The flow rate is controlled by the deflection and the frequency of the diaphragm's displacement. Passive valves are used for directing the flow. Poiseuille flow analogy is used to generate the equivalent pressure drop and flow rate via modifying the viscosity in the valve-channel in order to replace the variation of the channel width due to valve movement. Overall flow in the micropump is governed by three-dimensional time-dependent Navier Stokes equations. Deformation of the domain due to moving boundaries that coincide with the diaphragm motion is handled with the arbitrary Lagrangian-Eulerian method. Flow rate, hydraulic power and the efficiency of the micropump are obtained with respect to driving frequency and displacement of the diaphragm.

INTRODUCTION

Micropumps are in demand for a vast range of applications such as surgical operations [1], fuel delivery [2], electronic cooling of microdevices [3] and bio-chemical sensors and actuators [4]. Micropump designs vary with respect to their operation conditions and performance expectations [5]. Especially for liquids, viscous forces dominate the flow in micro scales limiting the transduction mechanisms that can be used in micropumps. In general, micropumps can be classified into two categories based on the principles of actuation that result in a net flow: (1) mechanical displacement pumps that utilize an actuated diaphragm or a similar moving part to generate pressure difference, and (2) dynamic pumps that utilize an electric or magnetic field, and ultrasonic waves on a boundary to generate an external force to move the fluid [5,6,7].

Mechanical reciprocating positive-displacement pumps, in general, consist of a diaphragm membrane or a piston, and at least one or two check valves or nozzle-diffuser type passive-components to move and direct the flow. High flow rates are obtained only with the application of large voltages to piezoelectric-material drivers. A few drawbacks of these mechanical pumps include complexity of the design, and unsteady flow rates. Producing controllable steady flows with mechanical micropumps remains somewhat a challenge.

Electrically conducting and magnetic fluids can be forced to flow by means of an external electric or magnetic field. However, the emerging electric currents in the fluid may not suitable for many applications.

Here, we present a micropump design composed of a dome-shaped diaphragm and two passive valves, which are attached to the inlet and exit of the pump as shown in Fig. 1. Circular diaphragm is placed at

the top of the cylindrical main chamber of the micropump. There are two rectangular channels attached to the main chamber, one is for the inlet and the other for the outlet. Each channel is restricted by a simple nozzle which has a flat restriction on one side and a gradual opening on the other side. Inside the opening of nozzles, prismatic parts are placed to form V-shaped channels. Prismatic parts are held with elastic tabs (not shown) that act as springs to limit the motion of the prismatic part. As the diaphragm moves into the chamber, the displaced fluid tries to escape from inlet and exit channels. The restrictions inside the channels cause a pressure build-up in the chamber, which is larger than the applied pressures at the inlet and the exit of the pump. Due to the pressure difference, inlet prism moves towards the inlet, and block the nozzle restricting the escaping fluid from the inlet; outlet prism, on the other hand, tends to clear the nozzle causing the fluid to escape more easily from the exit channel than the inlet channel. As the diaphragm moves outwards from the chamber forming a dome-shape, the pressure drop in the chamber causes to fluid to rush in from the inlet and exit ports causing both inlet and exit blocking prisms to move toward the chamber. At the exit port, the displacement of the prism will block the V-shaped channel further and restrict the back flow at the exit, the other prism at the inlet will open up to let the inlet flow fill in the chamber. Once the cycle completes, a net flow will emerge from the inlet to the outlet.

Due to large viscous forces Poiseuille flow conditions can be assumed in V-shaped channels at the inlet and exit of the pump. Thus the variation of the flow rate due to variation of the channel width and the pressure difference can be mimicked with the variation of an effective viscosity inside the V-shaped channel as explained further in the next section.

The motion of the diaphragm can be sustained by, for example, appropriate piezoelectric actuator rim which is placed at the edge of the diaphragm [8,9].

METHODOLOGY

The motion of the circular diaphragm is specified by the velocity of each point on the diaphragm along the z-axis:

$$w(r,t) = B\omega\cos(\omega t)(R^2 - r^2)/R^2 , \qquad (1)$$

where B is the maximum deflection of the center of the diaphragm, R is the radius of the diaphragm, r is the radial distance from the center of the diaphragm, $\omega = 2\pi f$ is the driving frequency and t is time. The general motion of the diaphragm is represented by the velocity vector, which is given by:

$$\begin{bmatrix} u \\ v \\ w \end{bmatrix} = \begin{bmatrix} 0 \\ 0 \\ w(r,t) \end{bmatrix}_{diaphragm} \qquad (2)$$

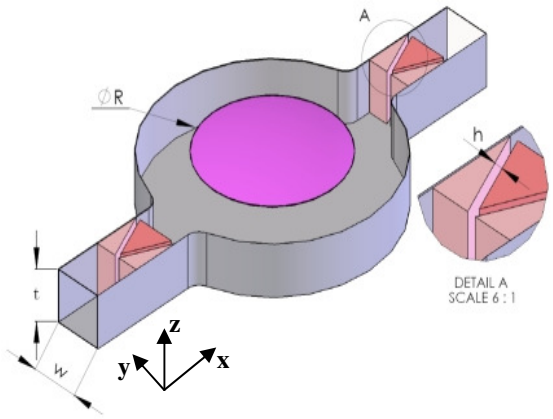

Figure 1: Three-dimensional view of the micropump and V-channels at the inlet and exit; inset shows a close-up view of the exit V-channel.

Incompressible Navier-Stokes equations subject to continuity govern the motion of the fluid in the time-varying domain, $\Omega(t)$, which is subject to the motion of the diaphragm boundary:

$$\rho\left(\frac{\partial \mathbf{U}}{\partial t} + (\mathbf{U} - \mathbf{u}_m)\cdot\nabla\mathbf{U}\right) = -\nabla P + \mu\nabla^2\mathbf{U} \qquad (3)$$

$$\nabla\cdot\mathbf{U} = 0 . \qquad (4)$$

In (3) and (4), $\mathbf{U}$ is the fluid velocity vector and $\mathbf{u_m}$ is the velocity of the moving coordinates due to the deformation of the domain with respect to initial stationary reference coordinate frame. Deforming domain inside the pump chamber is represented by the arbitrary Lagrangian-Eulerian (ALE) [10,11] method, which incorporates Winslow smoothing [12]. The velocity of the moving coordinates is specified by:

$$\mathbf{u_m} = \begin{bmatrix} 0 \\ 0 \\ w(z,t)(z/H) \text{ for } r < R \end{bmatrix} \qquad (5)$$

Essentially, Eq. (5) represents a rubber mesh deformation underneath the diaphragm in the chamber, where the local points get squeezed and stretch following the diaphragm's motion [13]; at the bottom of the chamber, z=0, domain deformation is specified as 0, and at the diaphragm, $z = H$ with respect to the initial coordinates, the velocity of the deformation is equal to the diaphragm's velocity given by Eq. (1).

Eqs. (3) and (4) are subject to no-slip boundary conditions at the chamber and channel walls, specified velocity, by (2) at the diaphragm, neutral flow conditions at the inlet and exit [11]:

$$\left[-P\mathbf{I}+\boldsymbol{\sigma}\right]\cdot\mathbf{n}\Big|_{in,t}=0 \tag{6}$$

$$\left[-P\mathbf{I}+\boldsymbol{\sigma}\right]\cdot\mathbf{n}\Big|_{out,t}=0\ , \tag{7}$$

where $\mathbf{n}$ is the surface normal vector and $\boldsymbol{\sigma}$ is the full stress tensor. In efficiency simulations, the inlet boundary condition is replaced with specified pressure.

Passive valve model

Motion of the passive valves is eliminated in this model to relieve the numerical burden of fluid structure interactions in V-shaped channels (gaps). Due to very low Reynolds number of the flow, one can assume Poiseuille flow conditions in V-channels for which the flow rate is specified as [14]:

$$Q \propto \frac{2h^3}{3\mu}\frac{\Delta P_{ch}}{\ell}\mathrm{t} \tag{8}$$

where Q is the flow rate, h is the V-channel height, t is the width, and ℓ is the V-channel length as depicted in (Fig. 1). The flow rate in Eq. (8) is a function of the channel height and pressure difference it is subjected to, i.e. $\Delta P_{ch}= P_{in} - P_{out}$, which corresponds to the pressure difference between the inside and outside the pump at the exit, and the pressure difference between the outside and inside the pump at the inlet.

Therefore, instead of modeling the motion of the prismatic valves in and out of the wedge, which effectively changes the V-channel height (gap thickness) and dictates the flow rate for a given pressure difference across the V-channels, the effective viscosity of the fluid within deforming channels can be used to mimic the varying gap thickness. This modification leads to the same flow rate for the given pressure difference, and is given by:

$$\frac{\mu_{ch}}{\mu_0}=\left(\frac{h_0}{h_{ch}}\right)^3 \tag{9}$$

where, h_0 and μ_0 are the unmodified height and viscosity of the fluid inside the V-channel for zero reference pressure difference, $\Delta P_{ch} = 0$, and h_{ch} and μ_{ch} are modified channel height and the modified viscosity corresponding to h_{ch}.

Furthermore, the displacement of the prism due to the pressure difference can be assumed as linear if springs attached to the prism are linear. Then, we also have:

$$\frac{h_{ch}}{h_0}=1-\frac{P_{in}-P_{out}}{\Delta P_{\max}} \tag{10}$$

where P_{in} and P_{out} are pressures at inlets and exits of V-channels respectively, and $\Delta P_{\max}$ is the maximum pressure which results in the collapse of the gap between the prism and wedge and preferably higher than pressures which are encountered in simulations, so as not to violate the linearity assumptions of springs (in Eq. (10)) and avoid unrealistic negative values for the channel effective-viscosity in Eq. (9).

Thus, from Eq. (8,9,10) the modified effective viscosity in V-channels can be determined from the pressure difference between inlets and exits of V-channels. Note that channel pressure difference at the inlet is negative of the pressure difference at the exit when both inlet and exit of the micropump is exposed to the same pressure boundary conditions. According to Eq. (10), when the chamber pressure is lower than outside, V-channel height at the inlet (exit) increases (decreases), and when the chamber pressure is higher than outside, then channel height at the inlet (exit) decreases (increases).

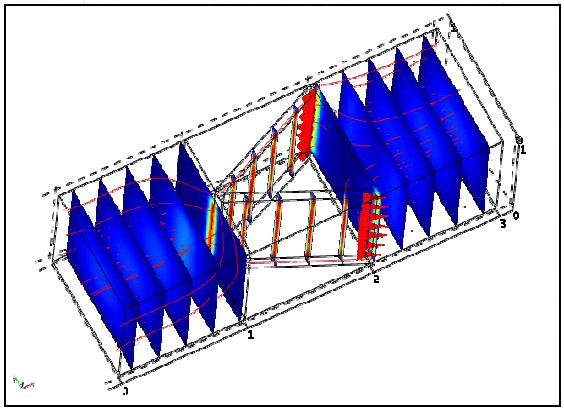

Figure 2: The simple valve used in testing of the Poiseuille-flow assumption and viscosity modification. Streamlines indicate the trajectory of fluid packets, 3D arrows (scaled with respect to the strength) show the flow direction. Sliced color surfaces correspond to the the x-velocity.

The validity of the Poiseuille flow approximation is tested for a flow inside a channel that contains a single valve, which is subject to zero inlet pressure and time-periodic outlet pressure (Fig. 2). The variation of the V-channel height (gap thickness) with the pressure difference between the inlet and outlet of the channel is specified according to Eq. (10). Time-averaged flow rates calculated from moving-valve and Poiseuille-flow-based modified viscosity simulations, and are compared in Fig. 3 for different frequencies of the exit pressure. For frequencies up to

1000 Hz, the time-averaged flow rates from modified-viscosity and moving prism simulations are nearly identical. Moreover, instantaneous flow rates are also observed to be nearly identical (not shown here). Thus, one can assume that modified-gap-viscosity assumption can be used safely instead of actually simulating the motion of prisms in passive valves.

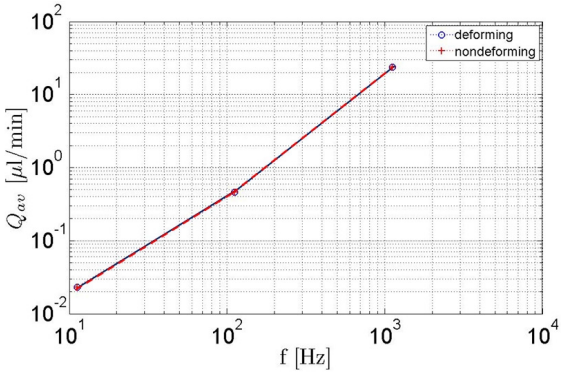

Figure 3: Time averaged flow rate for moving wedge (blue) and time averaged flow rate for stationary wedge (red).

Performance metrics

Instantaneous flow rate is determined from the integral of the *x*-velocity at the outlet of the pump:

$$Q(t) = \int_{A_{exit}} u(y,z,t)\,dA \tag{11}$$

Time-averaged flow rate is determined from last two-cycles of the simulations that correspond to two full-cycles of the diaphragm deformation, leading to:

$$Q_{av} = \frac{f}{2}\int_{t_o}^{t_o+2/f} Q(t)\,dt \tag{12}$$

Instantaneous rate of work done on the fluid (hydraulic power) by the moving diaphragm is calculated from the area integration of the product of the total *z*-stress and the local *z*-velocity, i.e.

$$\Pi(t) = \int_{A_{diaphragm}} \Sigma_z w(r,t)\,dA \tag{13}$$

where r is the position measured from the center of the diaphragm, Σ_z is the z-component of the full stress tensor, which is given by [16]:

$$\Sigma_z = \begin{bmatrix} \mu\left(\frac{\partial u}{\partial z}+\frac{\partial w}{\partial x}\right) \\ \mu\left(\frac{\partial v}{\partial z}+\frac{\partial w}{\partial y}\right) \\ \left(2\mu\frac{\partial w}{\partial z}-P\right) \end{bmatrix} \tag{14}$$

Similarly to Eq. (12), time-averaged hydraulic power is calculated by integrating the instantaneous power over the last two cycles of simulations:

$$\Pi_{av} = \frac{f}{2}\int_{t_o}^{t_o+2/f} \Pi(t)\,dt \tag{15}$$

Lastly, the efficiency of the micropump is determined by the ratio of the work-rate output of the pump to the time-averaged hydraulic power [17]:

$$\eta = \frac{\Delta P_{\text{pump,max}} Q_{\text{av,max}}}{4\Pi_{av}} \tag{16}$$

where $\Delta P_{pump,\max}$ is the maximum pressure head, $Q_{\text{av,max}}$ is the maximum flow rate that the pump can deliver. Note that $Q_{\text{av,max}}$ is essentially the average flow rate calculated from Eq. (12) from the simulations where the inlet and exit of the pump are subject to zero pressure boundary conditions.

RESULTS

Numerical simulations are carried out with the third-party software COMSOL, which utilizes the finite-element method. Simulations that are presented here are based on about 150000 degrees of freedom from about 12000 prismatic and 1500 hexahedral second order Lagrangian elements with first order pressure. Deformation velocity of the mesh, i.e. the Lagrangian strain-rate is calculated with the arbitrary Lagrangian-Eulerian method that utilizes Winslow smoothing in COMSOL. Linear systems coming out of finite-element discretization are solved with the PARDISO solver of the COMSOL along with Intel's MKL-BLAS libraries [15], which are invoked to take advantage of the automatic parallelization of the code. Each simulation takes between 1 to 3 hours on a double dual-core 3.7-GHz-Xeon workstation with 16GB of RAM running on SUSE Linux 10.0 operating system.

Effect of the deformation amplitude

In variable amplitude simulations, we use a non-dimensional geometry whose parameters are specified in Table 1.

Simulations are carried out using nondimensional amplitude which is given by:

$$B^* = B / L_0, \tag{17}$$

where L_0 is the length scale which corresponds to the height of the undeformed pump and its inlet and exit channels as specified in Table 2. Other characteristic scales used in variable amplitude runs are also specified in Table 2.

Geometric variables (dimensionless)	Value
Channel height, t^*	1
Inlet-exit channel width, w^*	1
Diaphragm radius, R^*	1.5
Deformation amplitude, B^*	0.1 (in constant amplitude simulations)
Driving frequency, f^*	1 (in constant frequency runs

Table 1. Default values for geometric variables used in simulations, unless otherwise noted

Characteristic scales in constant frequency simulations	Representative values
Length, L_0	$H = 10^{-3}$ m
Velocity, U_0	$Hf = .0112$ ms^{-1}
Time, t_0	$1/f = 0.0893$ s
Pressure, P_0	$\rho H^2 f^2 = 0.1254$ Pa
Flow rate, Q_0	$H^3 f = 1.12\times10^{-7}$ m^{3}s^{-1}
Hydraulic power, Π_0	$\rho H^5 f^3 = 1.4\times10^{-8}$ W

Table 2. Characteristic scales and their base values used in simulations and comparison of results. Here f is the driving frequency, and H is the dimensional height of the pump and its inlet and exit channels.

As the amplitude of deformations of the diaphragm increases, more fluid is displaced volumetrically and one expects a linear dependence between the flow rate and the amplitude as observed in Fig. 4. However, if the time-averaged flow rates are compared, we observe a quadratic dependence on the amplitude of the diaphragm deformation as shown in Fig. 5. In fact, this behavior manifest itself in Fig. 4, as the deformation amplitude increases, even though the maximum of the time-dependent flow remains nearly linear, amplitude of the backflow does not keep its linear dependence on the deformation amplitude. Thus the (im)balance indicates higher than first order increase of the time-averaged net-flow with the deformation amplitude.

In Figure 6, the effect of amplitude on hydraulic power (rate of work done on the fluid by the moving diaphragm) is plotted. Due to increasing vertical velocity of the diaphragm and increasing pressure in the chamber, the overall increase in the hydraulic power is quadratic with increasing deformation amplitude.

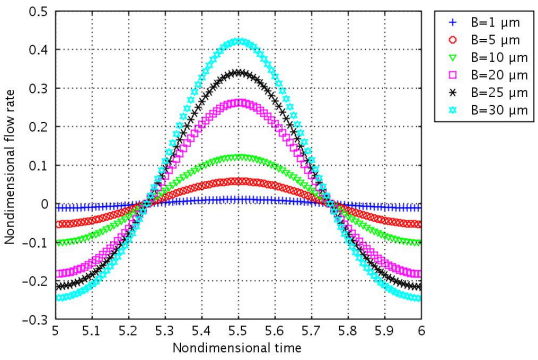

Figure 4: Time-dependent flow rate (at the exit) against non-dimensional time for which maximum displacement takes place at $t^* = 5.5$ in the plot. Amplitude of the flow rate increases linearly with the amplitude of deformations.

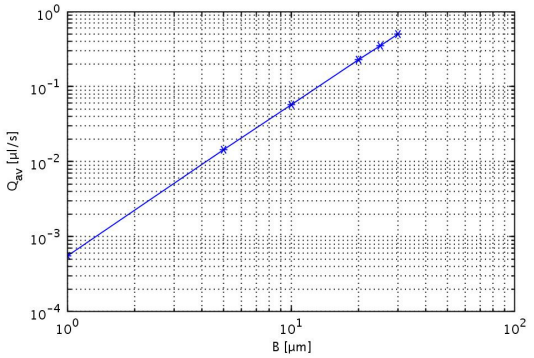

Figure 5: The effect of the amplitude of the diaphragm's deformation on time-averaged flow rate at the exit.

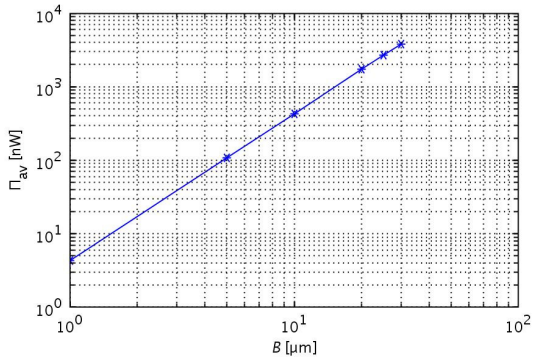

Figure 6: Effect of the deformation amplitude on the time-averaged hydraulic power.

Effect of the driving frequency

In variable frequency simulations, nondimensional time and the frequency in simulations are kept constant, as 1. The Reynolds number, which is given by Eq. (18) is varied in the simulations:

$$\mathrm{Re} = \frac{\rho L_0 U_0}{\mu}. \qquad (18)$$

Characteristic scales used in Eq. (18) and others are specified in Table 3 for constant amplitude, B = 100 μ, and variable frequency simulations.

Characteristic scales used in constant amplitude simulations	**Representative values**
Length, L_0 [m]	$H = 10^{-3}$
Velocity, U_0 [ms^{-1}]	$2\pi fB$
Time, $t_0 = L_0/U_0$ [s]	$H / 2\pi fB$
Pressure, P_0 [Pa]	$\rho\left(2\pi fB\right)^2$
Flow rate, Q_0 [m^{3}s^{-1}]	$H^2\left(2\pi fB\right)$
Hydraulic power, Π_0 [W]	$\rho H^2\left(2\pi fB\right)^3$

Table 3. Characteristic scales and their base values used in simulations and comparison of results. Here f is the driving frequency, and H is the dimensional height of the pump and its inlet and exit channels.

As shown in Fig. 7, the average flow rate varies quadratically with the driving frequency at relatively low frequencies. This behavior is somewhat counter intuitive, as one would expect a linear dependence between the frequency and the average flow rate. Simply put, as one doubles the number of deformation cycles with fixed amplitude in a fixed period of time, the total flow must also double; hence one must obtain twice as much flow rate. However, essentially, the same argument applies for the relationship between the flow rate and the amplitude (Figs. 4 and 5), yet we observe that, even though the time-dependent flow rate obeys to that argument, time-averaged flow rate deviates from the linear dependence due to the behavior of the passive valves. A similar behavior, is, thus, expected here.

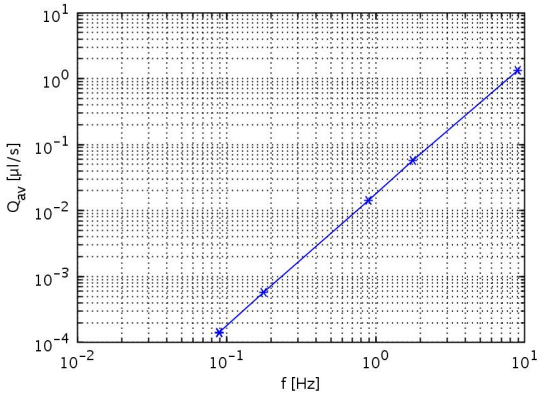

Figure 7: Driving frequency vs. time averaged flow velocity power consumption.

In Fig. 8, the variation of the hydraulic power with the varying frequency is depicted. The hydraulic power varies quadratically with the frequency. Hydraulic power has two components (see Eqs. (13) and (14)). As the frequency increases, so does the velocity and one would expect a proportional increase in the pressure as well. Thus, a quadratic dependence between the hydraulic power and the frequency is somewhat expected.

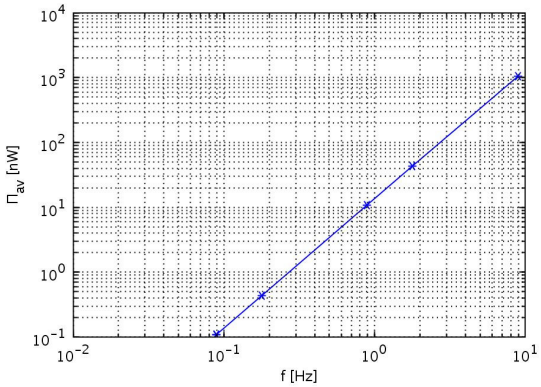

Figure 8: Driving frequency vs. time averaged hydraulic power consumption.

Efficiency of the micropump

To obtain the characteristic curves of the micropump, we carried out a number of additional simulations in which the inlet pressure is set to a negative value. We then computed the average flow rate using Eq. (12). As one would expect, typical characteristic curves which exhibit linear dependence between the flow rate and the pressure head are obtained. Thus, the efficiency of the pump can be calculated from Eq. (16).

The maximum pressure head is calculated from the characteristic curves by extracting the pressure head that corresponds to the zero time-averaged flow-rate. The maximum flow rate corresponds to the one for which the zero inlet and exit pressures are specified for the pump's inlet and exit, and are readily calculated from variable amplitude and frequency simulations.

In Fig. 9, the efficiency of the micropump is plotted against the deformation amplitude. For small amplitudes, the efficiency varies quadratically with the amplitude. However, one expects leveling-off of this behavior as the amplitude becomes large enough in comparison with the height of the pump.

In Fig. 10, the efficiency of the micropump is plotted against the driving frequency. According to the plot, for small frequencies the efficiency of the pump increases cubically with the frequency. Similar to the case for the varying amplitude, as the frequency becomes large enough the cubic increase of

efficiency must stall. Numerical problems are currently being sorted out to elucidate the behavior of the micropump for large amplitudes and frequencies.

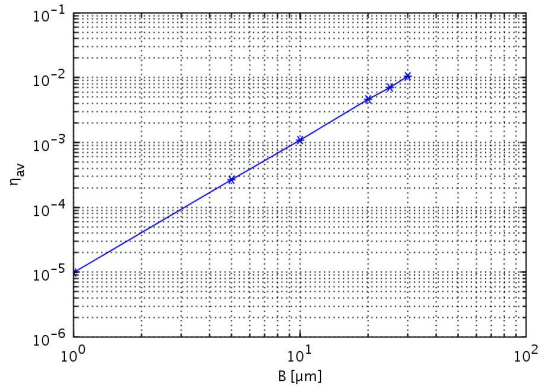

Figure 9: Efficiency of the micropump plotted as a function of deformation amplitude of the diaphragm.

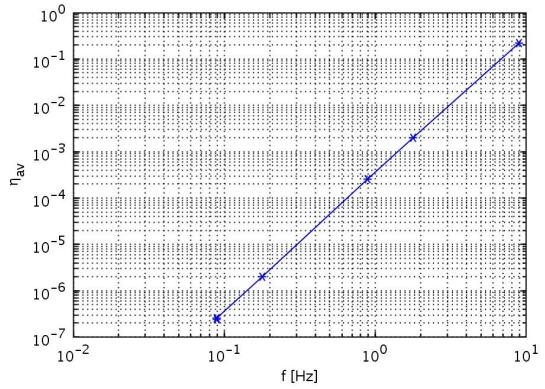

Figure 9: Efficiency of the micropump plotted as a function of drive frequency of the diaphragm.

CONCLUSIONS

A displacement-type micropump design is analyzed with respect to its operating conditions using simulation-based experiments. The micropump consists of a moving circular diaphragm which is placed at the top of a cylindrical chamber and two passive valves placed at the inlet and exit channels attached to the main chamber. Passive valves consist of prismatic parts attached to springs, and can move in and out of a V-shaped channel according to the pressure difference between the chamber and the inlet and outlet. The varying flow conditions due to the motion of prisms are modeled using Poiseuille flow assumption in the narrow channels between the prisms and V-channels. The viscosity of the fluid in the gap is modified to mimic the changing gap thickness.

The flow inside the micropump is modeled using time-dependent three-dimensional Navier-Stokes equations and arbitrary Lagrangian Eulerian method (ALE) in a deforming coordinate system due to motion of the diaphragm boundary. A number of simulations are carried out to determine the average flow rate, hydraulic power and the efficiency of the micropump as a function of the deformation amplitude and the driving frequency of the diaphragm.

According to simulation results, which concentrate on the small amplitude and small frequency part of the scale, the average flow rate and hydraulic power have quadratic dependence on both the amplitude and the frequency, i.e.

$$Q_{av} \sim \left(Bf\right)^2, \quad \Pi_{av} \sim \left(Bf\right)^2 \tag{19}$$

The efficiency of the micropump, which has a linear characteristic curve, varies quadratically with the amplitude and cubically with the frequency, i.e.

$$\eta_{av} \sim B^2 f^3. \tag{20}$$

Work is underway to elucidate the behavior of the micropump for large deformation amplitudes and drive frequencies of the diaphragm.

REFERENCES

[1] Mack, M.J., 2003, "Beating Heart Surgery: Does It Make a Difference?," The American Heart Hospital Journal, 1(2), pp. 149-157.

[2] Zhang, T., 2005, "Valveless Piezoelectric Micropump for Fuel Delivery in Direct Methanol Fuel Cell (DMFC) Devices," PhD Thesis Submitted to Graduate Faculty of the School of Engineering, University of Pittsburgh.

[3] Tuckerman, D. B., Pease, R.F.W., 1981, "High-Performance Heat Sinking for VLSI," IEEE Electron. Device Lett., 2, pp. 16-129.

[4] Garcia, M., Krimoama, S., Marlborough, D., Leafasia, J., Rieckmann, K.H., 1996, "Immunochromatographic Test for Malaria Diagnosis (letter)," Lancet, 347, pp.1549.

[5] Laser, D.J., Santiago, J.G., 2004, "A Review of Micropumps," J. Micromech. Microeng., 14, pp. R35-R64.

[6] Nguyen, N.T., White, R.M., 1999, "Design and Optimization of an Ultrasonic Flexural Plate Wave Micropump Using Numerical Simulation," Sensors and Actuators, 77, pp. 229-236.

[7] Lemoff, A.V., Lee, A.P., Miles, R.R., McConaghy, C.F., 1999, "An AC Magnetohydrodynamic Micropump: Toward a True Integrated Microfluidic

System," 10th International Conference on Solid-State Sensors and Actuators, Sendai, Japan.

[8] Piefort, V., Henrioulle, K., 2000, "Modelling of Smart Structures with Colocated Piezoelectric Actuator/sensor Pairs: Influence of the In-plane Components," Identification, Control and Optimization of Engineering Structures, Civil-Comp Press, Edinburgh UK.

[9] Piefort, V., 2001, "Finite Element Modelling of Piezoelectric Active Structures," PhD Thesis submitted to Faculty of Applied Sciences, PhD Thesis, Université Libre De Bruxelles.

[10] Duarte, F., Gormaz, R., Natesan, S., 2004, "Arbitrary Lagrangian-Eulerian Method for Navier-Stokes Equations with Moving Boundaries," Comput. Methods Appl. Mech. Engrg., 193, pp. 4819-4836.

[11] COMSOL, A.B., 2005, COMSOL Multiphysics User Guide.

[12] Winslow, A., 1967, "Numerical Solution of the Quisilinear Poisson Equations in a Nonuniform Triangle Mesh," J. Comp. Phys., 2, pp. 149-172.

[13] Tabak, A.F., 2007, "Simulation Based Experiments of Traveling-Plane-Wave-Actuator Micropumps and Microswimmers," MS Thesis submitted to Faculty of Engineering and Natural Sciences, Sabanci University.

[14] Kundu, P.K., Cohen, I.M., 2005, "Fluid Mechanics, Third Edition," Elsevier, Delhi, Chap. 15.

[15]http://www.intel.com/cd/software/products/asmo-na/eng/perflib/219780.htm, **2007.**

[16] Landau, L.D., Lifshitz, E.M., 2005, "Fluid Mechanics 2nd Ed.", Course of Theoretical Physics Vol. 6, Elsevier Butterworth-Heinemann, Oxford.

[17] Munson, B.R., Donald, F.Y., Okiishi, T.H., 2002, "Fundamentals of Fluid Mechanics 4th Ed.", John Wiley & Sons, Inc., USA.